






Proceedings Article

Image Time-Series Stability for MPI-Based Functional Neuroimaging

John M. Drago ^{a,b,*}, Erica E. Mason ^b, Eli Mattingly ^{b,c}, Monika Śliwiak ^b, Lawrence L. Wald ^{b,c}

^aDepartment of Electrical Engineering and Computer Science, MIT, Cambridge, MA, USA

^bMartinos Center for Biomedical Imaging, Massachusetts General Hospital, Boston, MA, USA

^cHarvard-MIT Health Sciences and Technology, Cambridge, MA, USA

*Corresponding author, email: jdrago@mit.edu

© 2022 Drago et al.; licensee Infinite Science Publishing GmbH

This is an Open Access article distributed under the terms of the Creative Commons Attribution License (<http://creativecommons.org/licenses/by/4.0>), which permits unrestricted use, distribution, and reproduction in any medium, provided the original work is properly cited.

Abstract

The temporal stability of an image time-series becomes a critical performance metric when magnetic particle imaging (MPI) is used as a functional neuroimaging modality. We apply an existing framework for assessing time-series variance from the functional MRI (fMRI) literature to phantom MPI time-series images. In this framework, sources of time-series variance are divided into those arising from thermal noise sources (which do not scale with the signal level) and intensity variations that scale with the signal level. The latter are often thought of as “physiological noise” if they arise from physiological processes or as instrumental “nuisance fluctuations” when arising from instrumental instabilities, such as system gain fluctuations. We analyze the time-series stability of a rodent-sized field-free line (FFL) MPI scanner during phantom imaging and assess the relative contributions of different noise sources to the time-series by varying the super-paramagnetic iron-oxide nanoparticle (SPION) concentration. These measurements permit characterization of our system’s time-series noise and suggest the signal levels at which the time-series will be dominated by instrumental instabilities rather than thermal noise or physiological modulations.

I. Introduction

Cerebral blood volume (CBV)-based functional neuroimaging modalities attempt to detect the approximate 20% blood volume changes that occur during neural activation [1]. Within this abstract, we describe a framework (from the fMRI literature) for time-series signal-to-noise ratio (SNR) metric quantification in MPI-based functional neuroimaging. We additionally demonstrate phantom imaging time-series stability and characterize the thermal and instrumental instability contributions for our existing small-animal imaging system.

I.1. The tSNR Formulation

The ratio of a pixel’s signal level to its intensity variation across a time-series of images is the principal signal-to-noise metric for time-series functional neuroimaging experiments. Following the terminology and analysis of Kruger and Glover [2], this metric, termed “tSNR”, is formed from the ratio of the pixel’s mean intensity, \bar{S} , to its standard deviation over time, defined as σ_{total} .

$$\text{tSNR} = \frac{\bar{S}}{\sigma_{\text{total}}} \quad (1)$$

In *in vivo* functional neuroimaging, “noise” in the time-series arises from both thermal noise, σ_0 , and also from noise sources whose variation increases in proportion to

the signal. Signal-level-dependent noise sources, σ_p , include instrument instabilities with a signal dependence and physiological signal modulation [3].

The SNR of an individual image due only to thermal noise, σ_0 , is defined:

$$\text{SNR}_0 = \frac{\bar{S}}{\sigma_0}. \quad (2)$$

Here, σ_0 is of thermal origin from coil or body losses or preamplifier noise. σ_p should ideally reflect signal modulation from physiological processes (such as respiration and cardiac activity). If these two “noise” sources are thought to be uncorrelated, then we can define the total time-series image noise, σ_{total} [2]:

$$\sigma_{\text{total}} = \sqrt{\sigma_0^2 + \sigma_p^2}. \quad (3)$$

The determination of the ratio of physiological noise to thermal noise can be derived by comparing measurements of SNR_0 and tSNR.

$$\frac{\sigma_p}{\sigma_0} = \sqrt{\left(\frac{\text{SNR}_0}{\text{tSNR}}\right)^2 - 1} \quad (4)$$

When σ_p can be described as a modulation of the signal, it is proportional to the signal level: $\sigma_p = \lambda \bar{S}$, with proportionality constant, λ . A direct relationship between SNR_0 and tSNR can then be formed.

$$\text{tSNR} = \frac{\text{SNR}_0}{\sqrt{1 + (\lambda \text{SNR}_0)^2}} \quad (5)$$

Equation 5 describes a system where the tSNR does not increase indefinitely as SNR_0 is improved, but approaches an asymptotic value of $1/\lambda$, as the image SNR (SNR_0) increases. Similar to the biological sources, instrumental gain variations over time could also contribute signal-level-dependent “noise” to phantom image time-series. It is desirable for these non-thermal instrumental variances to be insignificant compared to the unavoidable biological and thermal sources. When instrumental modulations that are proportional to \bar{S} are small, λ is near zero for phantom imaging, and the plot of tSNR vs. SNR_0 should be the identity line.

Operation of the scanner in a regime maximally sensitive to biological sources is especially important given that some biological sources are of interest. For example, metabolic fluctuations from neuronal firing, whose correlations form the basis of brain network analysis is a source of physiological noise. Physiological time-series variance that is proportional to signal level has been previously reported in resting rodent brain MPI signals [4], which is consistent with neuronal-driven CBV fluctuations. An instrumentation goal, therefore, is to create a time-series scanner whose λ in phantom data is sufficiently smaller than the expected λ value for *in vivo*

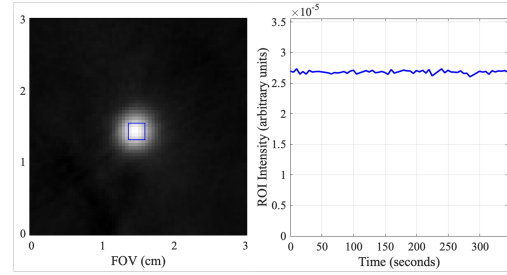


Figure 1: An example ROI for an 18 μl spherical glass bulb phantom with 5 μg Fe/ml Synomag®-D, and the mean of this ROI over the five-minute time-series with an image acquired every five seconds.

measurements. This would ensure that a given MPI system is capable of detecting the physiological “noise” of interest. We demonstrate the characterization of the λ free parameter for our system below.

II. Methods

The small-animal imager used for tSNR characterization has been detailed previously [5, 6]. The image resolution for this 2.83 T/m, mechanically-rotating FFL system is approximately 2.5 mm. A five-second image is formed from 27 projections, spanning 180 degrees. Sixty-six projection points are acquired at each angle to span a field of view of 30 mm. Image reconstruction was performed with an inverse Radon transform algorithm implemented on MATLAB (Mathworks, Natick, MA).

Multiple 18 μl glass bulbs phantoms were filled with PEG-coated 70 nm Synomag®-D (micromod, Germany) diluted in deionized water. Phantoms with iron concentrations spanning three orders of magnitude were used. The iron concentrations roughly reflect the expected *in vivo* concentrations of a rodent brain. If a 300 g rodent is injected with a 10 mg Fe/kg SPION dose, assuming rodent total blood volume of 64 ml/kg with 5% voxel blood volume [4], we expect a concentration of 7.88 μg Fe/ml in the brain. Thus, sensitivity to 1.6 μg Fe/ml is needed to detect a 20% blood volume change.

A 60-image time-series, comprised of five minutes of continuous, five-second images, was acquired for each imaging run. Following standard functional neuroimaging post-processing, a third-degree polynomial was fit to the acquired data, and low temporal frequency signal drift was removed from the time-series [7, 8]. To quantify the thermal noise that defines σ_0 , the standard deviation of an individual pixel was taken across all time points with no SPIONs in the imaging bore. σ_{total} and \bar{S} are measured by taking the standard deviation and mean, respectively, of a given pixel across the time-series. Metrics were averaged over a 5×5 pixel grid in the center of the glass bulb (Figure 1). The free parameter, λ , was

determined by using a nonlinear solver in MATLAB to fit the resultant tSNR and SNR_0 data to Equation 5.

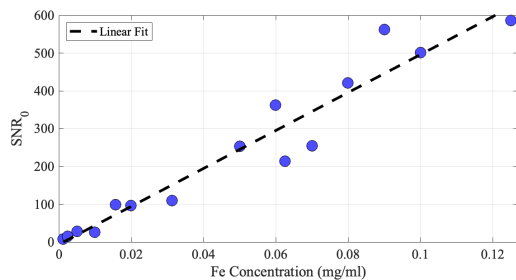


Figure 2: SNR_0 in a 5×5 phantom ROI vs. iron concentration. SNR_0 increases, as expected, with the concentration of iron. The R^2 for the plotted data, assuming a linear fit, is 0.93.

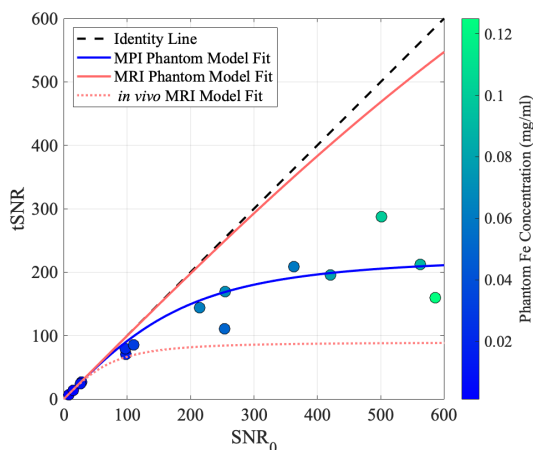


Figure 3: Plot of tSNR as SNR_0 increases. The λ parameter for the evaluated small-bore MPI phantom imaging system was $\lambda = 0.00444$. From MRI phantom measurements in the literature [3], $\lambda = 0.00075$ (red solid line), and from *in vivo* fMRI imaging, $\lambda = 0.0112$ (red dashed line).

III. Results

Figure 1 shows an example plot of the region of interest (ROI) mean over the time-series. Figure 2 shows a plot of SNR_0 as iron concentration increases. The plot exhibits the expected linear increase in signal as the iron concentration is increased. The resultant tSNR vs. SNR_0 plot for the phantom measurements is shown in Figure 3. Each point in the plot represents a different iron concentration, as indicated in the color bar. The λ determined by fitting Equation 5 to the measured data was 0.00444. Figure 3 demonstrates this model fit as a solid blue line.

IV. Discussion and Conclusion

We formalize and apply a framework to characterize the temporal stability of functional MPI (fMPI) systems. From the fMRI literature, the value of λ has been shown to change based on the imaging system used (e.g., 1.5 T vs. 3 T vs. 7 T), but the parameter value of λ for *in vivo* functional imaging is typically around $\lambda = 0.010$, whereas for a phantom, λ is on the order of $10\times$ lower: $\lambda = 0.0008$ [3]. The derived λ value from phantom imaging of our MPI system is 0.00444 – a higher instrumentation variation source than what is observed in fMRI. It will be important to determine whether different SPIONs produce varying λ values in phantom and *in vivo* imaging.

From Equations 4 and 5, the expected SNR_0 value that corresponds to a 1:1 ratio of σ_0 to σ_p in our system for phantom imaging was determined to be $\text{SNR}_0 = \frac{1}{\lambda} = 225$. For image SNR below this, sources of noise other than signal-level-dependent instrumental instabilities are expected to dominate. The *in vivo* SPION concentration for rodent imaging is expected to be on the order of $10 \mu\text{g Fe/ml}$, which corresponds to a phantom SNR_0 of approximately 26 in our system. At this SNR_0 , the σ_p to σ_0 ratio from instrumental sources is expected to be 11.5%. This ratio demonstrates that tSNR will be dominated by either thermal noise or genuine physiological fluctuations for our current imaging system at the expected *in vivo* SPION concentration and not by signal-level-dependent noise instabilities in the instrument. This motivates the use of the current system in rodent fMPI studies to characterize the noise contribution from physiological processes with *in vivo* rodent testing and ultimately determine the asymptotic limit of tSNR that can be achieved with *in vivo* brain fMPI.

Author's Statement

Authors state no conflict of interest.

References

- [1] T. Kim, K. S. Hendrich, K. Masamoto, and S.-G. Kim. Arterial versus total blood volume changes during neural activity-induced cerebral blood flow change: Implication for bold fmri. *Journal of Cerebral Blood Flow & Metabolism*, 27(6):1235–1247, 2007.
- [2] G. Krüger and G. H. Glover. Physiological noise in oxygenation-sensitive magnetic resonance imaging. *Magnetic Resonance in Medicine: An Official Journal of the International Society for Magnetic Resonance in Medicine*, 46(4):631–637, 2001.
- [3] C. Triantafyllou, R. D. Hoge, G. Krueger, C. J. Wiggins, A. Potthast, G. C. Wiggins, and L. L. Wald. Comparison of physiological noise at 1.5 t, 3 t and 7 t and optimization of fmri acquisition parameters. *Neuroimage*, 26(1):243–250, 2005.
- [4] C. Z. Cooley, J. B. Mandeville, E. E. Mason, E. T. Mandeville, and L. L. Wald. Rodent cerebral blood volume (cbv) changes during hypercapnia observed using magnetic particle imaging (mpi) detection. *Neuroimage*, 178:713–720, 2018.

- [5] K. Herb, E. Mason, E. Mattingly, J. Mandeville, E. Mandeville, C. Cooley, and L. Wald. Functional mpi (fmpi) of hypercapnia in rodent brain with mpi time-series imaging. *International Journal on Magnetic Particle Imaging*, 6(2 Suppl 1), 2020.
- [6] E. Mattingly, E. Mason, K. Herb, M. Śliwiak, K. Brandt, C. Cooley, and L. Wald. Os-mpi: An open-source magnetic particle imaging project. *International Journal on Magnetic Particle Imaging*, 6(2 Suppl 1), 2020.
- [7] A. M. Smith, B. K. Lewis, U. E. Ruttimann, Q. Y. Frank, T. M. Sinnwell, Y. Yang, J. H. Duyn, and J. A. Frank. Investigation of low frequency drift in fmri signal. *Neuroimage*, 9(5):526–533, 1999.
- [8] R. Kopel, R. Sladky, P. Laub, Y. Koush, F. Robineau, C. Hutton, N. Weiskopf, P. Vuilleumier, D. Van De Ville, and F. Scharnowski. No time for drifting: Comparing performance and applicability of signal detrending algorithms for real-time fmri. *NeuroImage*, 191:421–429, 2019.